11th International Conference on Vibration Problems
Z. Dimitrovová *et.al.* (eds.)
Lisbon, Portugal, 9–12 September 2013

# FLUID-STRUCTURE INTERACTION COUPLING ON FREE MOVING CYLINDERS IN LOW REYNOLDS NUMBER FLOWS

**João Luiz F. Azevedo*[1], Luiz Augusto C. A. Schiavo[2], Rafael N. Ihi[2], João Henrique A. Azevedo[2], William R. Wolf[3]**

[1]Instituto de Aeronáutica e Espaço, DCTA/IAE/ALA, São José dos Campos, SP, 12228-903, Brazil
joaoluiz.azevedo@gmail.com

[2]Instituto Tecnológico de Aeronáutica, DCTA/ITA, São José dos Campos, SP, 12228-900, Brazil
augustoschiavo@gmail.com, rafael.ihi@hotmail.com, joaohenrique.azevedo@gmail.com

[3]Universidade Estadual de Campinas, UNICAMP, Campinas, SP, 13083-970, Brazil
wolf@fem.unicamp.br

**Keywords:** Vortex Induced Vibration, Fluid-Structure Interaction, CFD, Free and Forced Oscillations.

**Abstract.** *Vortex-induced vibration (VIV) is of practical interest in many fields of engineering, and is widely evident in aerospace and naval fields. This problem of fluid-structure interaction is easily found in risers, transmission lines and launch vehicles at the launch ramp, for example, and it is capable of influencing the dynamics of these structures. The long term objective of the work here reported is to develop the capability of analyzing fluid-structure interaction problems on oil-platform risers using CFD techniques. The specific aspects discussed in the present work concern validation of a computational tool and the study of a model fluid-structure interaction problem relevant in this case. This model problem considers the 2-D flow over a cylinder which is free to move in the longitudinal and transversal directions. The cylinder is restrained by linear springs which have their stiffness constants calculated in such a way to yield natural oscillating frequencies that correspond to representative oscillating frequencies of actual risers. Mass ratios for the fluid-structure interaction are selected to be consistent with actual values for the riser problem. The flows of interest are assumed to be adequately modeled by the 2-D Reynolds-averaged Navier-Stokes equations, with appropriate turbulence closures. In particular, most of the tests included in the present work have used the Spalart-Allmaras turbulence model. The CFD code used is a finite volume code originally developed for treating aeroelastic problems for typical aerospace applications, which has been adapted for the present low speed problems. The study addresses forced motions of the cylinder as well as free moving cases. In both cases, the present results are compared to literature data as well as computations performed using commercial codes. The flow Reynolds number, based on the cylinder diameter, is varied from 300 to 10,000. The present results are in good agreement with the available data for similar flow configurations. Nonetheless, one can observe that the lack of inclusion of three-dimensional effects has strong influence on the results if the Reynolds number is considerably increased.*

## 1 INTRODUCTION

Vortex-induced vibration (VIV) is a particular case of the fluid-structure interaction phenomenon that affects many fields of engineering and has been the subject of a large number of investigations, such as the work in Refs. [1, 2, 3, 4, 5]. There is a larger availability of data for low Reynolds numbers ($Re$), while, for higher values of this parameter, it becomes increasingly more difficult to find reliable data. One of the most studied cases of VIV is the flow around a free cylinder, due to its practical applications concerning the dynamics of oil risers, chimney towers, high voltage cables and antennae, among others. The first lift measurement on a circular cylinder was carried out by [6], that recorded the wall pressure around an underwater cylinder with $Re = 110{,}000$. Recent efforts to predict the lift and drag coefficients of an oscillating cylinder under prescribed displacement, using numerical simulations were made by [7] and [8], using direct numerical simulation (DNS). Nonetheless, the literature lacks lift and drag measurements for a freely vibrating cylinder, with few exceptions, such as Ref. [9], that conducted a two degree of freedom experiment for $Re \cong 6{,}000$.

The present work is focused on the numerical investigation of the fluid-structure interaction of a flow over a cylinder, and the validation of a CFD tool through the comparison between the aerodynamic coefficients of an oscillating circular cylinder and results of the literature. The cylinder is considered to be elastically mounted and rigid, undergoing either forced or free oscillation. In the former case, the body is restrained to move transversely or longitudinally with respect to the flow, by a prescribed harmonic displacement of moderate amplitude. In the latter case, the cylinder is free to move only in the crossflow direction and its motion is governed by a structural-dynamic equation. Moreover, the influence of Reynolds number and flow velocity on the aerodynamic coefficients of the cylinder are analyzed.

## 2 THEORETICAL AND NUMERICAL FORMULATION

### 2.1 Theoretical formulation

The CFD tool used in this work is based on the 2-D Navier-Stokes equations, which represent a two dimensional flow of compressible viscous fluid through a continuous medium in transient regime. In a finite volume approach, these equations can be written in Cartesian form as

$$\frac{\partial}{\partial t}\int_{V_i} Q dx dy + \oint_{S_i} (E dy - F dx) = 0\,. \tag{1}$$

In Eq. (1), $V$ represents the control volume or the area, and $S$ is the length of the edges of the element. The $Q$ variable is a vector of conserved properties, and the $E$ and $F$ variables are the flux vectors in the $x$ and $y$ directions, respectively. These variables are written as

$$Q = \left[\ \rho \quad \rho u \quad \rho v \quad e\ \right]^T\,, \tag{2}$$

$$E = E_e + E_v \qquad \text{and} \qquad F = F_e + F_v\,. \tag{3}$$

Here, $E_e$ and $F_e$ represent the inviscid flux, or Euler flux, and $E_v$ and $F_v$ represent the viscous terms. The Euler fluxes are

$$E_e = \left\{ \begin{array}{c} \rho U_c \\ \rho u U_c + p \\ \rho v U_c \\ (e+p)U_c + x_t p \end{array} \right\}, \qquad F_e = \left\{ \begin{array}{c} \rho V_c \\ \rho u V_c \\ \rho v V_c + p \\ (e+p)V_c + y_t p \end{array} \right\}. \tag{4}$$

In the previous equations, $U_c$ and $V_c$ are the contravariant velocity components, which, in unsteady cases, take into account the mesh velocity components $x_t$ and $y_t$ as

$$U_c \,=\, u \,-\, x_t \,, \quad V_c \,=\, v \,-\, y_t \,. \tag{5}$$

The viscous flux vectors are written as

$$E_v \,=\, \left\{ \begin{array}{c} 0 \\ \tau_{ii} \\ \tau_{ji} \\ \tau_{ii}u \,+\, \tau_{ji}u - q_j \end{array} \right\} \,, \qquad F_v \,=\, \left\{ \begin{array}{c} 0 \\ \tau_{ij} \\ \tau_{jj} \\ \tau_{ij}v \,+\, \tau_{jj}v - q_j \end{array} \right\} \,. \tag{6}$$

The nomenclature employed here is usual in the CFD community, where $\rho$ is density or specific mass, $u$ and $v$ are the Cartesian velocity components in the x and y directions, respectively, $e$ is the total energy, $p$ is the pressure, $\tau_{ij}$ are the components of the viscous stress tensor in Einstein's notation, $\mu$ is the molecular dynamic viscosity coefficient, $\delta_{ij}$ is the Kronecker delta operator, and $\lambda$ is the volumetric viscosity coefficient which is defined by the Stokes hypothesis. As such, $\tau_{ij}$ and $\lambda$ are written as

$$\tau_{ij} \,=\, \mu \left( \frac{\partial u_i}{\partial x_j} \,+\, \frac{\partial u_j}{\partial x_i} \right) \,+\, \lambda \frac{\partial u_k}{\partial x_k} \delta_{ij} \,, \qquad \lambda \,=\, -\,\frac{2}{3}\mu \,. \tag{7}$$

Finally, the heat flux, $q_i$, is obtained by Fourier's law of heat conduction, where $K$ is the coefficient of thermal conductivity,

$$q_i \,=\, -\,K \frac{\partial T}{\partial x_i} \,. \tag{8}$$

### 2.2 Spatial and time discretizations

The numerical scheme adopted in this work is a cell centered finite volume method. The discrete value of conserved flow field vector variables is computed for the $i$-th control volume as

$$Q_i \,=\, \frac{1}{V} \int_{V_i} Q dV \,, \tag{9}$$

where $Q_i$ is the mean value of $Q$ in the instant of time $t$, for the control volume $V_i$. Equation (1) can be rewritten for each $i$th cell as

$$\frac{\partial Q_i}{\partial t} \,=\, -\int_{S_i} \left( E dy \,-\, F dx \right) \,. \tag{10}$$

According to [10], for each control volume face, flux information of flow field variables must be computed from $i$-th and $n_b$-th control volumes which share a $k$-th face. Hence, the flux computation is built as

$$\int_{s_i} \left( E dy \,-\, F dx \right) \approx \sum_{k=1}^{s_i} \left[ E\left(Q_k\right) \left( y_2 \,-\, y_1 \right) \,-\, F\left(Q_k\right) \left( x_2 \,-\, x_1 \right) \right] \,. \tag{11}$$

The $E\left(Q_k\right)$ and $F\left(Q_k\right)$ fluxes are computed by a prescribed value, $Q_k$, at the $k$-th face. The flux computation is, then, accordingly distributed between $i$-th and $n_b$-th control volumes. Moreover, all variables or parameters necessary at face are computed by a simple averaged procedure,

$$Q_k \,=\, \frac{1}{2} (Q_i \,+\, Q_{nb}) \,. \tag{12}$$

Thus, the inviscid and viscous fluxes can be written for each control volume as

$$C\left(Q_i\right) \;=\; \sum_{k=1}^{nf} \left[E_e\left(Q_k\right)\left(y_2 \,-\, y_1\right) \,-\, F_e\left(Q_k\right)\left(x_2 \,-\, x_1\right)\right] \,, \tag{13}$$

$$V\left(Q_i\right) \;=\; \sum_{k=1}^{nf} \left[E_v\left(Q_k\right)\left(y_2 \,-\, y_1\right) \,-\, F_v\left(Q_k\right)\left(x_2 \,-\, x_1\right)\right] \,. \tag{14}$$

Furthermore, since the spatial discretization is centered, artificial dissipation terms must be added. In the present case, these terms are represented by the $D(Q_i)$ operator, which is the algebraic nonlinear artificial dissipation operator proposed in Ref. [10].

The second-order accurate, five-stage, explicit hybrid Runge-Kutta scheme proposed by [11] and by [12] is adopted for the time discretization. This scheme can be written as

$$\begin{aligned} Q_i^{(0)} \;&=\; Q_i^n \,, \\ Q_i^{(j)} \;&=\; \frac{V_i^n}{V_i^{n+1}} Q_i^{(0)} \,-\, \Theta_j \frac{\Delta t_i}{V_i^{n+1}} \left[C\left(Q_i^{(j-1)}\right) \,-\, D\left(Q_i^{(j-1)'}\right) \,-\, V\left(Q_i^{(0)}\right)\right] \,, \\ Q_i^{n+1} \;&=\; Q_i^{(5)} \,, \end{aligned} \tag{15}$$

Although the present work considers a mesh moving rigidly with the body, this scheme already includes the necessary terms to account for changes in cell area due to deformation of the mesh [12]. Values for the $\Theta_j$ coefficients can be seen in Ref. [10].

### 2.3 Turbulence model and meshing considerations

As previously discussed, the structural model considered in the present work is a 2-D cylinder section. The test cases are simulated as laminar or turbulent flows, given that the current Reynolds number range of interest is in the lower end of the range in which transition occurs. When running a turbulent case, the Spalart-Allmaras turbulence model [13] is used. This model requires less computational efforts to be solved because, by construction, less refined meshes are required near wall surfaces, when compared, for instance, to the more stringent mesh needs for some two equations models. The meshes used in the present work are generated with the ICEM CFD© commercial grid generator.

The dynamic system represented in the cylinder section is a rigid body with a plunge degree of freedom, transversal to the flow. Unsteady calculations involve body motion and, therefore, the computational mesh and boundary conditions should be somehow adjusted to take this motion into account. Two approaches are adopted here in order to create such movement. The first approach is to prescribe the motion as part of the input of the simulation. Prescribed motions consist of sinusoidal functions. The idea of this approach is to validate the numerical solver through frequency content analysis. On the other hand, the second method is to integrate a structural-dynamic formulation coupled to the fluid dynamics solver. In the present free cylinder model, the stiffness of the beam-like cylinder is represented by a linear spring. The dynamics of the mass-spring system with a natural frequency $\omega$ can, then, be written as

$$\frac{d^2\bar{y}}{d\bar{t}^2} + \left(\frac{\omega}{\omega_r}\right)^2 \bar{y} = \frac{2C_L}{\pi\mu_r} \,. \tag{16}$$

Moreover, $\mu_r$ is the mass ratio and $\omega_r$ is a reference frequency conveniently selected. The previous equation is, then, marched in time using a standard 4th-order, 4-stage Runge-Kutta method.

The far-field boundary conditions are adjusted in order to account for the motion as reported in [14]. In the present work, the authors have selected to move the mesh rigidly with the inner boundary. This approach is less computationally expensive than employing a deformable mesh, with a fixed outer boundary, that accommodates for the movement of the inner boundary. Regardless of the type of motion being calculated, the mesh velocity components can be calculated as

$$x_{t_j} = \frac{x_j^{n+1} - x_j^n}{\Delta t}, \qquad \text{and} \qquad y_{t_j} = \frac{y_j^{n+1} - y_j^n}{\Delta t}. \tag{17}$$

The new cell areas are determined employing the geometric conservation law concept [15], where the total area conservation is imposed in a similar manner to the flow variables.

## 3 RESULTS AND DISCUSSION

### 3.1 Fixed cylinder analysis

Tests with a fixed cylinder were performed with the purpose of evaluating the accuracy of the present formulation in the analysis of a low Reynolds number flow. Simulations are performed at $Re = 300$, where the Reynolds number is defined in terms of the cylinder diameter. Results for the drag coefficient are compared with the literature in Table 1. This includes the experimental data from Mittal and Balachandar [16] and the results of Lima e Silva *et al.* [7], that performed DNS calculations for the same configuration. The other data included in Table 1 are extracted from [7].

| Present work | Lima e Silva et al. | Park et al. | Sucker & Brauer | Ye et al. | Mittal & Balachandar |
|---|---|---|---|---|---|
| 1.20 | 1.27 | 1.37 | 1.22 | 1.38 | 1.22 |

Table 1: Mean drag coefficients for a Reynolds number 300 flow over a circular cylinder.

Results at $Re$ = 1,000 are shown in Table 2. Strouhal number, $S_t$, lift coefficient, $C_L$, and mean and maximum drag coefficients, calculated in the present work, are compared to a two-dimensional compressible RANS simulation [5]. All properties analyzed have good correlation with the literature data. It is important to notice that [5] used a formulation that is similar to the present work. The cited paper solves the compressible, viscous, 2-D Navier-Stokes equations without turbulent modeling, as in the present case. These comparisons indicate that the current code yields results which are consistent with the data in the literature.

| Property | Reference | Present Work | Difference (%) |
|---|---|---|---|
| $C_\ell$ | 1.365 | 1.364 | 0.1 |
| $C_{d_{\text{mean}}}$ | 1.462 | 1.414 | 3.3 |
| Ampl. $C_d$ | 0.188 | 0.185 | 1.5 |
| $C_{d_{\text{max}}}$ | 1.652 | 1.599 | 3.2 |
| $St_{\text{calc.}}$ | 0.239 | 0.235 | 1.8 |

Table 2: Aerodynamic properties for the flow over a circular cylinder at $Re$ = 1,000.

### 3.2 Prescribed motion analysis

Results for a prescribed motion in the crossflow direction, with a moderate amplitude of 0.3 diameters, are compared to those from the commercial software CFD++©. Test cases are simulated with dimensionless frequency $(f_0 d)/U = 0.14$ and Reynolds number $Re = 1,000$. A prescribed sinusoidal motion, given by $Y(t) = A \sin(2\,\pi\, f_0\, t)$, is imposed to the cylinder. Table 3 shows the values of the rms lift and mean drag coefficients obtained. It is observed that the maximum error is only 7%, which demonstrates the good accuracy of the results. As the lift and drag coefficients undergo large changes in time, these coefficients are converted to the frequency domain, through the fast Fourier transform (FFT). The comparison of the magnitude and the frequency content of the unsteady lift and drag coefficients, for both CFD tools, can be visualized in Fig. 1. As noticed from this figure, the corresponding coefficient results show a very good correlation between the solutions with the two different codes. In other words, the spectra of lift and drag coefficients are in good agreement.

| Coefficient | In-house Code | CFD++ | Difference (%) |
|---|---|---|---|
| $C_{d_{\text{mean}}}$ | 1.478 | 1.594 | 7 |
| $C_{\ell_{\text{rms}}}$ | 0.985 | 1.034 | 5 |

Table 3: Comparison of aerodynamic coefficients for the prescribed motion test case for a $Re$ = 1,000 flow over a cylinder.

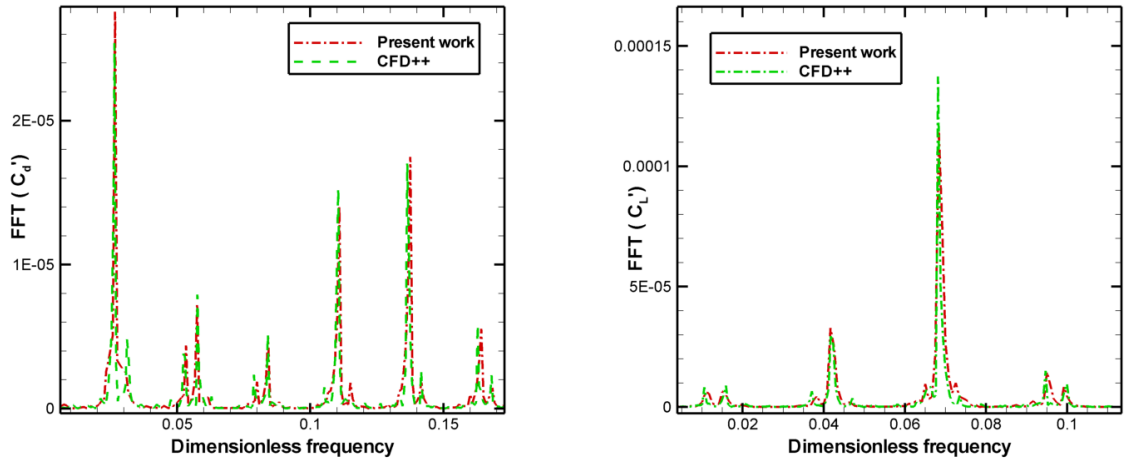


(a) Drag coefficient response.

(b) Lift coefficient response.

Figure 1: Frequency content of the aerodynamic coefficients for a $Re$ = 1,000 flow over a cylinder with prescribed motion.

Additional test cases address flows with a fixed Reynolds number of 10,000, but with different forcing frequencies. As $Re = 10{,}000$ lies in the transition range, simulations are carried out assuming laminar flow and, also, using the Spalart-Allmaras turbulence model [13]. The test cases and their results are summarized in Table 4. The present results are compared to the DNS data of [8] and the empirical results of [17] in Fig. 2. The calculations using the turbulence model yield a better comparison to the reference data, for most cases. Drag coefficients,

| Case | $Re$ | Amplitude $(Y/d)$ | $f_0U/d$ | $C_{d_{\text{mean}}}$ | $C_{\ell_{\text{rms}}}$ |
|---|---|---|---|---|---|
| M1 | 1,000 | 0.3 | 0.14 | 1.478 | 0.985 |
| M2 | 10,000 | 0.3 | 0.14 | 1.623 | 1.288 |
| M3 | 10,000 | 0.3 | 0.17 | 1.624 | 1.184 |
| M4 | 10,000 | 0.3 | 0.21 | 1.598 | 1.546 |
| M5 | 10,000 | 0.3 | 0.25 | 1.511 | 1.804 |
| M6 | 10,000 | 0.3 | 0.30 | 1.750 | 1.825 |

Table 4: Transversal oscillation results.

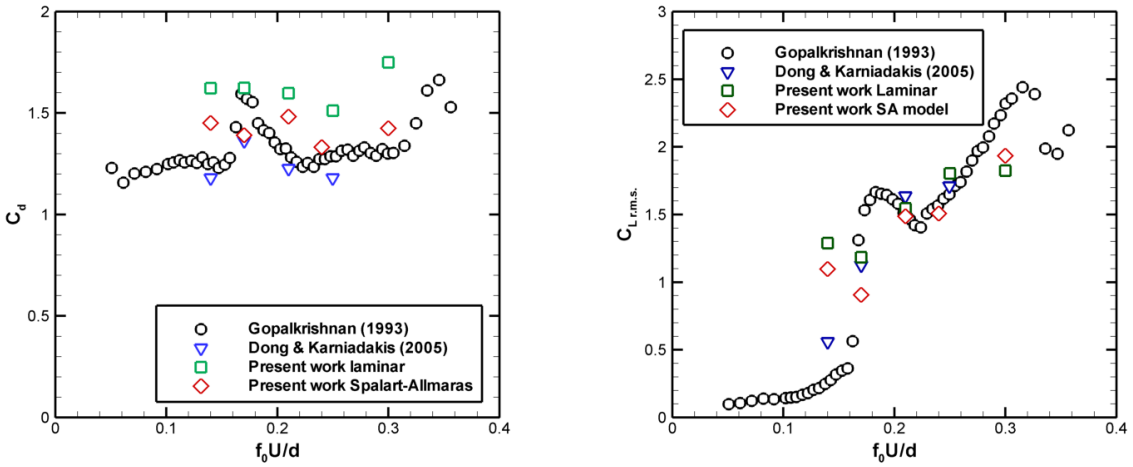


(a) Drag coefficient.

(b) Lift coefficient.

Figure 2: Comparison of the aerodynamic coefficients for a prescribed cylinder oscillation at $Re$ = 10,000.

for both laminar and turbulent calculations, are slightly over-predicted and the lift coefficients are under-predicted for the highest frequencies. Overall, the results are reasonably close to the literature, with the exception of the M2 case. A possible reason for this behavior is that the frequency for the M2 case is in a range of frequencies in which the coefficients go through a sharp increase and are, therefore, more susceptible to error. Moreover, the present work performs 2-D simulations while the cited references use 3-D configurations. Reference [18] indicates that the onset of 3-D instabilities, such as vortex formation in the spanwise direction, occurs for $Re > 200$. As indicated, these 3-D effects are not accounted for in the present work. A few simulations with forced oscillation in the longitudinal direction were also conducted. The agreement with the literature data is similar to what has been seen in the previous comparisons.

### 3.3 Free motion analysis

The simulations for free motion are conducted in such a way that, initially, calculations are performed for a fixed cylinder until the aerodynamic solution reaches a periodic state. This state provides the initial condition for the free cylinder calculations. Then, the cylinder is allowed to oscillate in the transversal direction by the influence of the aerodynamic forces. From this point on, the structure is considered to be constrained by linear springs in order to model the cylinder stiffness. The frequency response ratio is defined as $f^* = f/f_n$, where $f$ is the body oscillation frequency. The reduced velocity is expressed by $U^* = (2\pi U)\,/\,(f_n d)$, where $d$ is the cylinder

diameter, $U$ is the freestream velocity, and $f_n$ is the natural frequency of the structure.

Figure 3 (a) illustrates the behavior of the frequency response ratio, $f^*$, as a function of the reduced velocity, $U^*$. The results are indicating that, with the increase of reduced velocity, the vortex shedding frequency becomes closer to the natural frequency of the system and, hence, the two frequencies synchronize. This is the well known definition of the lock-in phenomenon [19]. The onset of the lock-in is characterized by a resonance and a hysteresis which was first demonstrated by [20]. As illustrated in Fig. 3 (b), in the lock-in region, the amplitude undergoes a sharp increase. The behavior of $f^*$ in the synchronization regime is similar to what is reported in the experimental work of [9] for low mass ratios. The results for dimensionless amplitude, $A^* = A_{max}/d$, as a function of the reduced velocity, are compared in Fig. 3 (b) to 2-D and 3-D DNS and experimental results obtained by [21]. Three response branches are clearly observed from this plot: the initial excitation, the upper and the lower branches.

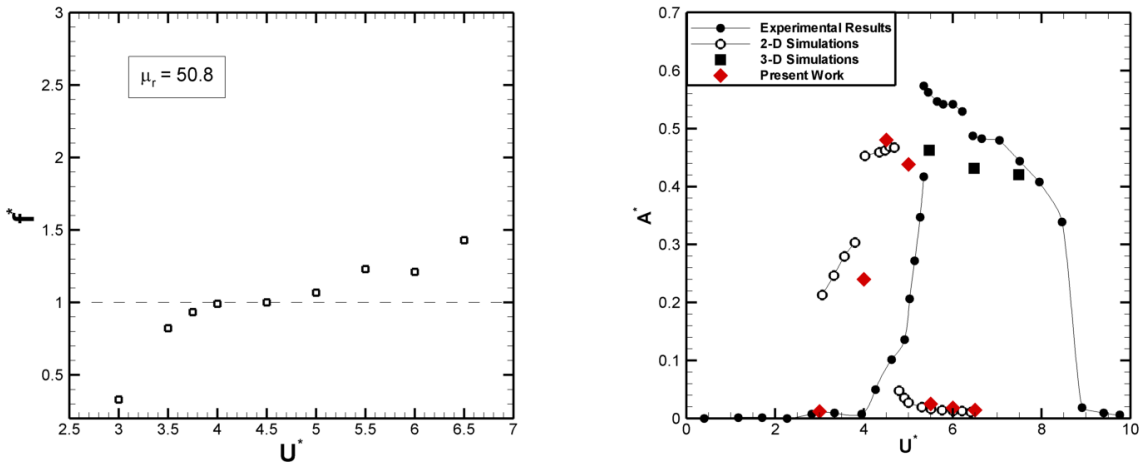


(a) Frequency response ratio.

(b) Dimensionless amplitude.

Figure 3: Frequency ratio and peak amplitude results for a $Re$ = 556 flow over a free oscillating cylinder.

Both the experimental data and the 3-D simulation results exhibit reasonable correlation, differently from the 2-D ones. Although one expects certain discrepancies between 2-D and 3-D simulations, because of the aforementioned three-dimensional effects, the difference observed is much more significant than anticipated. This fact is also corroborated by Table 5 that shows peak amplitude data for 2-D and 3-D calculations and experimental results, obtained by various authors. The peak amplitudes obtained in 2-D simulations are substantially under-predicted when compared to the 3-D calculation results, as well as being incapable of accurately estimating the response branches. Figure 3 (b) also shows that there is good agreement between the 2-D results of [21] and the present work, especially in the range $4.5 < U^* < 6.5$. Although the agreement between the results is not as good in the $3 < U^* < 4$ range, it is fair to state that there is good overall correlation between the 2-D results.

## 4 CONCLUDING REMARKS

The present work has analyzed fluid-structure interaction problems, namely vortex induced vibration, using CFD techniques. Simulations are conducted with a 2-D viscous solver developed in-house and it is shown that the code is capable of providing results which are in

| Author | Method | $Re$ | $m^*\zeta$ | $A^*$ |
|---|---|---|---|---|
| [22] | Experimental | 3,800 | 0.04 | 0.80 |
| [23] | Experimental | 6,000 – 35,000 | 0.052 | 0.95 |
| [24] | Experimental | 14,410 – 50,380 | 0.036 | 1.01 |
| [21] | Numerical 3-D | 556 | 0 | 0.46 |
| [25] | Numerical 2-D | 100 | 0 | 0.59 |
| [21] | Numerical 2-D | 556 | 0 | 0.47 |
| Present work | Numerical 2-D | 556 | 0 | 0.48 |

Table 5: Peak amplitude data for a free oscillating cylinder.

agreement to those obtained in similar studies. The configuration addressed here is a 2-D circular cylinder, which is considered to represent a section of a long cylindrical pipe subjected to a crossflow. The flow conditions studied in the present paper consider a Reynolds number range such that $300 < Re < 10,000$. Even thought the Reynolds number range of the present investigation lies in the lower end of the laminar-turbulent regime transition, the calculations using the Spalart-Allmaras turbulence model provided much more accurate results than laminar simulations of the prescribed motion test case. Free vibration results, for the present 2-D simulations, do not have good comparison with the 3-D calculations or experimental data from the literature. However, the present free vibration results do provide good overall correlation with other 2-D literature results.

## ACKNOWLEDGMENTS

The authors acknowledge the partial support received from CNPq, under Grants No. 312064/2006-3 and No. 471592/2011-0. Partial support for this research was also provided by FAPESP, under Grant No. 2013/07375-0. Further partial support provided by CAPES and FUSP is also gratefully acknowledged.

## REFERENCES

[1] T. Sarpkaya, Vortex-induced oscillations: A selective review. *Journal of Applied Mechanics*, **46**, 241–258, 1979.

[2] O.M. Griffin and S.E. Ramberg, Some recent studies of vortex shedding with application to marine tubulars and risers. *Journal of Energy Resources Technology*, **104**, 2–13, 1982.

[3] R.D. Blevins, *Flow-induced vibrations*. Van Nostrand Reinhold, New York, 1st edition, 1990.

[4] C.H.K. Williamson, Vortex dynamics in the cylinder wake. *Annual Review of Fluid Mechanics*, **28**, 477–539, 1996.

[5] A. Rohde, Numerical investigation of the evolution of vortex instability in a 2-D compressible flow over a cylinder. AIAA Paper No. 2011-3550. *20th AIAA Computational Fluid Dynamics Conference*, AIAA, Honolulu, Hawaii, 2011.

[6] H. Drescher, Messung der auf querangeströmte zylinder ausgeübten zeitlich veränderten drücke. *Zeitschrift für Flugwissenschaften und Weltraumforschung*, **4**, 17–21, 1956.

[7] A.L.F. Lima e Silva, A. Silveira-Neto, and J.J.R. Damasceno, Numerical simulation of two-dimensional flows over a circular cylinder using the immersed boundary method. *Journal of Computational Physics*, **189**, 351–370, 2003.

[8] S. Dong and G.E. Karniadakis, DNS of flow past a stationary and oscillating cylinder at Re = 10000. *Journal of Fluid and Structures*, **20**, 519–531, 2005.

[9] A. Khalak and C.H.K. Williamson, Motions, forces and mode transitions in vortex-induced vibrations at low mass-damping. *Journal of Fluids and Structures*, **13**, 813–851, 1999.

[10] D. Mavriplis, Accurate multigrid solution of the Euler equations on unstructured and adaptative meshes. *AIAA Journal*, **28**, 213–221, 1990.

[11] A. Jameson and D. Mavriplis, Finite-volume solution of the two-dimensional Euler equations on a regular triangle mesh. *AIAA Journal*, **24**, 611–618, 1986.

[12] J.T. Batina, Unstructured grid methods development – lessons learned. *Proceedings of the 4th International Symposium on Computational Fluid Dynamics*, Davis, CA, 1991.

[13] P.R. Spalart and S.R. Allmaras, A one-equation turbulence model for aerodynamic flows. *La Recherche Aerospastiale*, **1**, 5–21, 1994.

[14] A.N. Marques and J.L.F. Azevedo, Numerical calculation of impulsive and indicial aerodynamic responses using computational aerodynamics techniques. *Journal of Aircraft*, **45**, 1112–1135, 2008.

[15] P.D. Thomas and C.K. Lombard, Geometric conservation law and its application to flow computations on moving grids. *AIAA Journal*, **17**, 1030–1037, 1979.

[16] R. Mittal and S. Balachandar, On the inclusion of three-dimensional effects in simulations of two-dimensional bluff-body wake flows. *Proceedings of the ASME Summer Meeting, Symposium on Separated Complex Flows*, Vancouver, Canada, 1997.

[17] R. Gopalkrishnan, Vortex-induced forces on oscillating bluff cylinders. Ph.D. Thesis, Department of Ocean Engineering, Massachusetts Institute of Technology, Cambridge, MA, 1993.

[18] J. Wu, J. Sheridan, M.C. Welsh, and K. Hourigan, Three-dimensional vortex structures in a cylinder wake. *Journal of Fluid Mechanics*, **312**, 201–222, 1996.

[19] C.H.K. Williamson and R. Govardhan, Vortex-induced vibrations. *Annual Review of Fluid Mechanics*, **36**, 413–455, 2004.

[20] C. Feng, The measurement of vortex-induced effects in flow past stationary and oscillating circular and D-section cylinders. Master's Thesis, University of British Columbia, Vancouver, BC, Canada, 1968.

[21] H.M. Blackburn, R.N. Govardhan, and C.H.K. Williamson, A complementary numerical and physical investigation of vortex-induced vibration. *Journal of Fluids and Structures*, **15**, 481–488, 2000.

[22] F.S. Hover, A.H. Techetand, and M.S. Triantafyllou, Forces on oscillating uniform and tapered cylinders in crossflow. *Journal of Fluid Mechanics*, **363**, 97–114, 1998.

[23] H.M. Blackburn, R.N. Govardhan, and C.H.K. Williamson, Hydrodynamic damping, flow-induced oscillations, and biharmonic response. *Journal of Offshore Mechanics and Arctic Engineering*, **117**, 232–238, 1995.

[24] A.L.C. Fujarra, J.R. Meneghini, C.P. Pesce, and P.H.C.C. Parra, An investigation of vortex-induced vibration of a circular cylinder in water. *Proceedings pf the Conference on Bluff Body Wakes and Vortex-Induced Vibrations*, Washington, DC, 1998.

[25] D. Shields, A. Leonard, and A. Roshko, Flow-induced vibration of a circular cylinder at limiting structural parameters. *Journal of Fluids and Structures*, **15**(1), 3–21, 2001.